NJC

PAPER

Cite this: *New J. Chem.*, 2015, 39, 8006

High activity of aluminated bifunctional mesoporous silica nanoparticles for cumene hydrocracking and measurement of molar absorption coefficient†

Mohammad Reza Sazegar,*[ab] Sugeng Triwahyono,[b] Aishah Abdul Jalil,[c] Rino R. Mukti,[d] Seyed Mohammad Seyed Mohaghegh[ef] and Madzlan Aziz[b]

Received (in Montpellier, France) 5th June 2015,
Accepted 30th July 2015

DOI: 10.1039/c5nj01433f

www.rsc.org/njc

Bifunctional mesoporous silica nanomaterials (MSN) with various Si/Al molar ratios of 7, 10, 20 and 50 in platinum supported (Pt/HAlMSN) were synthesized using sol–gel methods followed by post-synthesis methods. XRD and nitrogen sorption results confirmed the mesoporous structure with surface areas of 537–775 $m^2\ g^{-1}$. ^{27}Al NMR spectroscopy confirmed aluminium loading with tetrahedral, pentahedral and octahedral structures. Pyridine adsorption IR results indicated that incorporation of aluminium led to the generation of strong Brønsted and Lewis acidic sites. Catalytic activity was investigated for cumene hydrocracking in a pulse microcatalytic reactor in the temperature range of 323–573 K which revealed that this activity depends on the number of Lewis and Brønsted sites. The high yield of cumene conversion increased from Si/Al molar ratios of 50 to 10 and decreased for the Si/Al molar ratio of 7 due to the presence of pentahedral Al and/or inactive tetrahedral Al atoms in Pt/HAlMSN-7. The high selectivity of α-methylstyrene showed the important role of Lewis acid sites in these bifunctional catalysts. In spite of the coke formation in the Pt/HAlMSN catalysts, reactivation recovered the activity of the catalysts after 100 h of reaction. The molar absorption coefficients of Pt/HAlMSN were measured using pyridine followed by water adsorption monitored by FTIR.

Introduction

Mesoporous silica nanoparticles (MSN) with specific characteristics like large surface area, large pore size and volume, catalytic behavior and adsorption properties open up many potential applications in catalysis, environmental protection and nanostructured materials.[1–3] Aluminium loading into MSN in order to produce active sites results in a decrease of the pore structure as compared with the pure MSN.[4] Protonation of mesoporous materials changes the pore structure as well as causes an undesirable loss of the 4-coordinated aluminium structure and appearance of the 6-coordinated aluminium structure.[5] Introduction of platinum into mesoporous silica materials usually combined with metal oxides such as Zr, Ir, Al and Mo oxides[6–8] was found to increase the catalytic activity. The protonation process can be applied to increase the amount and strength of acidic sites through the generation of Brønsted acid sites.

Recently, Jana *et al.*[9] synthesized Al-MCM-41 (Mobil Composition of Matter No. 41) catalysts with different molar ratios of Si/Al *via* four different synthesis methods: hydrothermal, grafting, sol–gel and template cation exchange. They showed that the acidity and catalytic activity increased with the increase of Al loaded into the catalyst structure. Al-MCM-41 showed the highest activity in the cracking reaction in comparison with zeolite Y, SBA-15 (Santa Barbara Amorphous 15) and ZSM-5 (Zeolite Socony Mobil-5) due to the highest acidity of Al-MCM-41.[10] Handjani *et al.*[11] synthesized Pt/Al-SBA-15 catalyst and showed that lower amount of Brønsted acid sites and higher amount of Lewis acid sites had an influence on the activity of the catalyst in cumene cracking.

Whereas few studies have been reported on the synthesis of Al-containing and platinum supported on mesoporous silicates, this study focused on the synthesis and characterization of protonated AlMSN with platinum supported in the cracking reaction. MSN exhibits a low catalytic activity due to the presence of weak Lewis acid sites and the absence of Brønsted acid sites in its framework. Incorporation of aluminium followed by protonation

[a] *Dept. of Chemistry, Fac. of Science, North Tehran Branch, Islamic Azad University, Tehran, Iran. E-mail: m_r_sazegar@yahoo.com; Tel: +98-2122262564*
[b] *Dept. of Chemistry, Fac. of Science, Universiti Teknologi Malaysia, 81310 UTM Johor Bahru, Johor, Malaysia*
[c] *Institute Hydrogen Economy, Dept. of Chemical Eng., Fac. of Chemical Eng., Universiti Teknologi Malaysia, 81310 UTM Johor Bahru, Johor, Malaysia*
[d] *Division of Inorganic and Physical Chemistry, Fac. of Mathematics and Natural Sciences, Institut Teknologi Bandung, Jl Ganesha No 10, Bandung 40132, Indonesia*
[e] *Dept. of Chemical Engineering and Applied Chemistry, University of Toronto, Toronto, ON, Canada*
[f] *Dept. of Polymer Science, Iran Polymer and Petrochemical Institute, Tehran, Iran*
† Electronic supplementary information (ESI) available. See DOI: 10.1039/c5nj01433f

generates strong Lewis and Brønsted acid sites which lead to an increase in the catalytic activity. In the present work, Pt/HAlMSN catalyst with different Si/Al ratios of 7–50 was synthesized and the cumene hydrocracking reaction was investigated in order to evaluate the effect of Al concentration accompanied by platinum species on cumene conversion. We report here the synthesis of MSN by a sol–gel method and incorporation of aluminium with different Si/Al ratios of 7, 10, 20 and 50 followed by protonation resulting in HAlMSN which was found to enhance the acidity, activity and stability of MSN. Platinum loading of HAlMSN (denoted Pt/HAlMSN) was carried out with as much as 0.1 wt% Pt which promoted the active sites for cumene hydrocracking reaction. The physical properties of Pt/HAlMSN were confirmed by nitrogen physisorption, XRD, FTIR, pyridine-FTIR and ^{29}Si and ^{27}Al solid state NMR. The activity of the Pt/HAlMSN catalysts was examined using the cracking of cumene under a hydrogen atmosphere. The conversion results revealed that the activity of the catalysts was strongly related to the number of Lewis and Brønsted acid sites. The role of platinum particles and Brønsted and Lewis acid sites in the formation of propene, benzene, toluene and α-methylstyrene in cumene cracking reaction was discussed in detail.

Experimental

The preparation method

General procedure for Pt/HAlMSN synthesis. The synthesis of MSN was carried out according to the previously reported procedure.[2] The mesoporous MSN was prepared using 1,2-propanediol (PD) as a co-solvent by a sol–gel method. Cetyltrimethylammonium bromide (CTAB, 1.17 g) was dissolved in an aqueous solution containing double distilled water (180 g) and 1,2-propanediol (PD, 30 mL) in an aqueous ammonia solution (7.2 mL, 25%). After vigorous stirring for approximately 30 min at 323 K, tetraethyl orthosilicate (TEOS, 1.43 mL) and 3-aminopropyl triethoxysilane (APTES, 0.263 mL) were added to the mixture. The resulting mixture was stirred for an additional 2 h at 323 K and allowed to rest for 20 h at the same temperature. The gel composition used in the synthesis of the parent MSN was 1TEOS : 0.17APTES : 0.5CTAB : 13.5NH_3 : 85.2PD : 1042H_2O.

The sample was collected by centrifugation for 30 min at 20 000 rpm and washed with deionized water and absolute ethanol 3 times. The surfactant was removed by heating MSN (1 g) in an NH_4NO_3 (0.3 g) and ethanol (40 mL) solution at 333 K. The surfactant-free product was collected by centrifugation and dried at 383 K overnight prior to calcination in air at 823 K for 3 h. The acidic sites of the samples were prepared by aluminium grafting on the template-free MSN at 353 K for 10 h followed by centrifugation and drying at 383 K overnight prior to calcination in air at 823 K for 3 h. Sodium aluminate (Sigma-Aldrich) was used as a precursor of aluminium. Al-grafted MSN was denoted as AlMSN. The initial molar ratios of Si/Al were 7, 10, 20 and 50. The AlMSN samples were synthesized by adding MSN (1 g) into an aqueous solution (50 mL) of sodium aluminate (0.154, 0.110, 0.054 and 0.022 g) for Si/Al ratios of 7, 10, 20 and 50, respectively, at 353 K for 10 h followed by centrifugation and drying at 383 K overnight prior to calcination in air at 823 K for 3 h with a heating rate of 1 K min^{-1}. The protonated AlMSN (HAlMSN) sample was synthesized by protonation of AlMSN (1 g) using aqueous solution of NH_4NO_3 (2.5 g in 50 mL of double distilled water) at 333 K for 16 h followed by removal of solution, drying at 383 K overnight and calcination at 823 K for 3 h in air. The Pt/HAlMSN catalysts were prepared by impregnation of HAlMSN with 0.1 wt% Pt solution followed by calcination in air at 823 K for 3 h. Chloroplatinic acid hydrate ($H_2PtCl_6{\cdot}6H_2O$, Sigma-Aldrich) was applied as a source of platinum.

Catalyst characterization. The crystallinity of catalysts was measured with a Bruker Advance D8 X-ray powder diffractometer with Cu Kα (λ = 1.5418 Å) radiation as the diffracted monochromatic beam at 40 kV and 40 mA. Nitrogen physisorption analysis was conducted on a Quantachrome Autosorb-1 at 77 K. Before the measurement, the sample was evacuated at 573 K for 3 h.

The elemental analysis of the catalysts was carried out using a Bruker S4 Explorer X-ray fluorescence spectrometer (XRF) using R_h as the anode target material operated at 20 mA and 50 kV. XRF analysis showed that the Si/Al ratios of the Pt/HAlMSN frameworks were 5.6, 9.0, 18.9 and 48.7 for S_7, S_{10}, S_{20} and S_{50}, respectively.

Fourier transform infrared (FTIR) measurements were carried out using an Agilent Carry 640 FTIR spectrometer. The catalyst was prepared as a self-supported wafer and activated under H_2 stream (F_{H_2} = 100 mL min^{-1}) at 623 K for 3 h, followed by in vacuum at 623 K for 1 h.[2,7] To determine the acidity of the catalysts, the activated samples were exposed to 2 Torr pyridine at 423 K for 30 min, followed by evacuation at 473 K for 1 h to remove physisorbed pyridine on the samples. In order to study the effect of activation temperature, the Pt/HAlMSN was activated at four different temperatures of 473, 523, 573 and 623 K. All spectra were recorded at room temperature. All spectra were normalized using the overtone and combination vibrations of the lattice of MSN between 2200 and 1300 cm^{-1} after activation, particularly the lattice peaks at 1855 cm^{-1}.[2] The number of Brønsted and Lewis acid sites was calculated using the integrated molar adsorption coefficient values.

The measurement of molar absorption coefficients of the catalysts was carried out by using IR spectroscopy. In this method the infrared experiments were carried out using 50 mg of sample pressed into a 15 mm diameter disk. Spectra were recorded after the initial evacuation of the sample at 673 K for 1 h and then after exposure to 1 Torr pyridine and evacuation at 423 K for 15 min, followed by outgassing at the same temperature. The IR spectrum was recorded at room temperature. Then, an amount of 5 Torr of water was introduced into the sample at 423 K for 2 h. After this period, FTIR spectra were recorded at room temperature with the integrated areas of the bands at 1455 and 1545 cm^{-1} due to the 19b ring vibrations of pyridine adsorbed at Lewis and Brønsted sites, respectively. The molar absorption coefficient and the value of Brønsted and Lewis acid sites were measured by exposure to 1 Torr of pyridine at 423 K for 15 min and outgassing at the same temperature, followed by adsorption of 1 Torr excess pyridine at 423 K for 20 min without followed by outgassing. Then, the IR spectrum was recorded at room temperature.

^{29}Si MAS NMR spectra were recorded on a Bruker Avance 400 MHz spectrometer at 79.49 MHz with 18 s recycle delays and spun at 7 kHz to determine the chemical status of the Si in the silicate framework of catalysts. ^{27}Al MAS NMR spectra were recorded at 104.3 MHz with 0.3 s recycle delays and spun at 7 kHz to determine the chemical status of aluminium in the silicate framework of catalysts.[12]

Catalytic activity. Hydrocracking of cumene was carried out under atmospheric pressure in a microcatalytic pulse reactor coupled with an online 6090N Agilent FID/TCD gas chromatograph equipped with a VZ-7 packed column. About 0.2 g of the catalyst was placed in an OD 10 mm quartz glass reactor and subjected to air (F_{Air} = 100 mL min^{-1}) stream for 1 h and hydrogen (F_{H_2} = 100 mL min^{-1}) stream for 4 h at 623 K.[2] A dose of cumene (36 μmol) was injected over the catalyst at the reaction temperature and the products were trapped at 77 K before flushing out to the gas chromatograph. In order to find the appropriate condition of cumene cracking, the reaction was done in the different temperature range of 323–523 K.

The cumene conversion (X_{cumene}) and selectivity of the products (S_i) were calculated according to eqn (1) and (2), respectively:

$$X_{cumene}(\%) = \frac{C_{in} - C_{out}}{C_{in}} \times 100\% \quad (1)$$

$$S_i(\%) = \frac{C_i}{(\sum C_i) - C_{cumene}} \times 100\% \quad (2)$$

where C_{in}, C_{out}, C_i and C_{cumene} are the mole number of cumene in the inlet, outlet, particular compound and residual cumene, respectively, which were calculated based on the Scott hydrocarbon calibration standard gas (Air Liquide America Specialty Gases LLC). i is the number of particular carbon.

Results and discussion

Preparation of catalyst

The parent MSN was synthesized through the sol–gel technique and the Pt/HAlMSN samples were prepared by aluminium loading of MSN followed by introduction of platinum. XRD patterns of the Pt/HAlMSN samples with Si/Al molar ratios of 50 to 7 are given in Fig. 1. An intense diffraction peak (100) at a low angle degree between 2θ = 2.28–2.40° and two small signals (110, 200) at 2θ = 4–5° were observed. The peaks confirmed the presence of two-dimensional hexagonal ($p6mm$) structure with a d_{100}-spacing of approximately 3.6 nm. Incorporation of aluminium into MSN reduced the order of hexagonal mesoporous structures significantly.[1] The shift in the peak position from 2.28° to 2.40° may be due to the substitution of Si atoms with larger atomic radius Al atoms which led to an increase in the interplanar spacing of MSN.

Table 1 shows the physical characteristics of Pt/HAlMSN catalysts with Si/Al ratios of 50 to 7. The surface areas are 775, 620, 537 and 361 m^2 g^{-1} for Pt/HAlMSN-50 to Pt/HAlMSN-7, respectively, which indicates the loading of aluminium on the catalyst surfaces. A decrease in the surface area showed a direct relationship with Al content which led to changes in the pore size distribution of catalysts which was probably due to the presence of extra-framework aluminium (EFAl) inside the pore.[13] ^{27}Al MAS NMR spectra confirmed the presence of an octahedral Al atom in the Pt/HAlMSN catalyst structure. The grafting of MSN with sodium aluminate caused plugging of the pores of MSN with a diameter around 3.5–4 nm (Fig. 2B). The plugging of the MSN increased with the increase in Al loading which led to a decrease in the pore size and volume (Table 1). The aluminium species were placed inside and/or on the mouth of the pores.[2] An increase in Al loading decreased the pore volume from 0.40 to 0.15 cm^3 g^{-1} and the pore size from 3.77 to 3.64 nm. The wall-thickness increased with Al incorporation from 0.47 to 0.56 nm while it decreased to 0.40 nm in Pt/HAlMSN-7. This decrease indicated that aluminium and residual sodium were placed inside and outside of the pores in the Al-rich sample with a Si/Al ratio of 7.

Similar results had been reported on aluminium immobilized mesoporous MCM-41 by Chen *et al.*[14] The introduction of

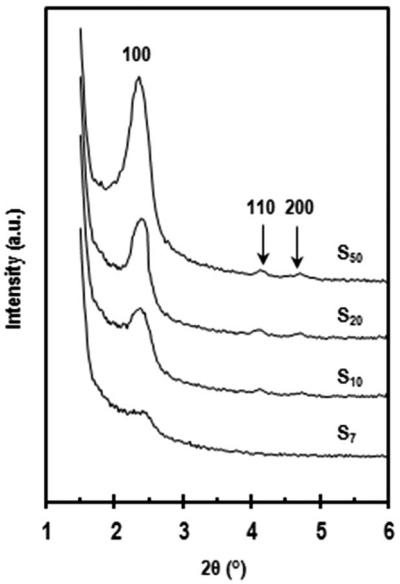

Fig. 1 XRD patterns of the Pt/HAlMSN catalysts with the Si/Al molar ratio of 7–50.

Table 1 Physical characteristics of the Pt/HAlMSN catalysts

Catalyst	d_{100} (nm)	a_0 (nm)	S (m^2 g^{-1})	V_p (cm^3 g^{-1})	W (nm)	t (nm)	Si/Al (exp.)	Si/Al (XRF anal.)
Pt/HAlMSN-7	3.50	4.04	361	0.15	3.64	0.40	7	5.6
Pt/HAlMSN-10	3.65	4.21	537	0.18	3.65	0.56	10	9.0
Pt/HAlMSN-20	3.59	4.15	620	0.29	3.67	0.48	20	18.9
Pt/HAlMSN-50	3.67	4.24	775	0.40	3.77	0.47	50	48.9

d_{100}, d-value 100 reflections; a_0, pore center distance is equal to $2d_{100}/\sqrt{3}$; S, BET surface area (m^2 g^{-1}) obtained from N_2 adsorption; V_p, total pore volume (cm^3 g^{-1}), W, pore size (nm) obtained from the BJH method, t, pore wall thickness is equal to $a_0 - W$; Si/Al (exp.), experimental Si/Al molar ratio; Si/Al (XRF anal.), Si/Al molar ratio analysed by XRF.

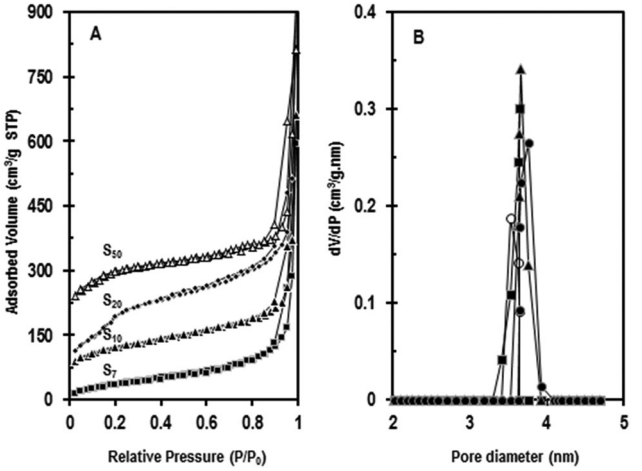

Fig. 2 (A) Nitrogen adsorption–desorption isotherms and (B) pore size distribution for Pt/HAlMSN with Si/Al of 7 (○), 10 (■), 20 (▲) and 50 (●).

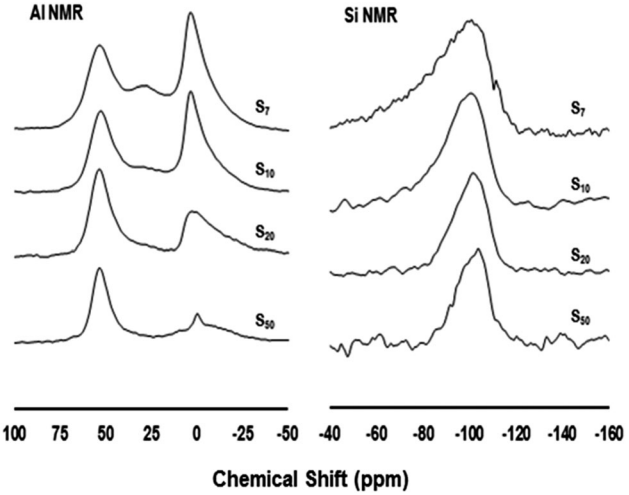

Fig. 3 ^{29}Si NMR and ^{27}Al MAS NMR of the Pt/HAlMSN catalysts with Si/Al ratios of 7–50.

aluminium into MCM-41 decreased the surface area from 1151 to 336 m^2 g^{-1} for Al-MCM-41 with Si/Al ratios of 15.3 to 1.9, respectively.

In addition, the presence of platinum in Pt/HAlMSN was investigated by using FESEM-EDX images and XRF analysis (ESI,† Appendices S1 and S2).

Fig. 2A and B exhibit nitrogen adsorption–desorption isotherms and the corresponding pore size distribution of Pt/HAlMSN catalysts which was calculated by the NLDFT method. The nitrogen sorption isotherm patterns of the samples exhibit type IV isotherms with H1-type hysteresis loops for all samples which is attributed to the mesoporous silica with uniform cylindrical pores (Fig. 2A).

The isotherms of catalysts show an inflection characteristic of capillary condensation at a relative pressure of $0.1 < P/P_0 < 0.3$, which displays the characteristic of porous structures with small and uniform mesopores.[15] A significant increase at higher relative pressure in the range of 0.8–1.0 indicates the presence of a textural porosity which is owing to the less ordered mesoporous structure due to the loading of Al into the pure mesoporous silica materials. An increase in Al loading slightly altered the properties of the sample. The presence of Al species plugged inside the micropores of the catalysts led to a decrease in the inflection at $P/P_0 < 0.2$ and a decrease in the intensity of pore size distribution.

In agreement with the results of nitrogen physisorption and XRD patterns, Subhan and co-workers[16] loaded Al over MCM-41 by a post-synthesis method with various Si/Al molar ratios ranging from 30 to 50. The XRD patterns showed an ordered hexagonal structure for the Al-MCM-41 samples. The BET results revealed a decrease in the surface area from 925 to 556 m^2 g^{-1} and a decrease in the pore volume from 0.60 to 0.49 cm^3 g^{-1} and no significant variation in pore size distribution was observed.

Fig. 3 shows the ^{29}Si MAS NMR and ^{27}Al MAS NMR spectra of the Pt/HAlMSN catalysts. The chemical shift of ^{29}Si NMR in aluminosilicates depends on the number of Al atoms in coordination with Si atoms and the peaks became broader with increasing Al concentration. The mesoporous silica materials consist of a significant proportion of silanol groups, which decrease with the alumination process. Typically, the chemical shift is about −110 ppm for $Si(OSi)_4$ units.[17] The corresponding signals overlap with those of Q^2 and Q^3 species, which makes it difficult to estimate the extent of aluminium from ^{29}Si NMR spectra. ^{29}Si NMR spectra of the series of exchanged samples are clearly shifted from −104 ppm for Pt/HAlMSN-50 to −97 ppm for Pt/HAlMSN-7. This confirms that the fraction of Si(OAl) species increased due to substitution of more Al into the mesoporous silica walls which is ascribed to $AlO–Si(OSi)_3$ and/or $HO–Si(OSi)_3$, $(AlO)_2–Si(OSi)_2$ and/or $(HO)_2–Si(OSi)_2$ sites. This result is in excellent agreement with the evolution of tetrahedral Al structure.[17]

In ^{27}Al MAS NMR spectra, the signal at 53 ppm described the presence of tetrahedrally (T_d) coordinated aluminium framework and a small peak at 28 ppm depicted pentahedral Al species and the peak at 0 ppm was assigned to octahedrally (O_h) coordinated aluminium non-framework.[10] This indicates that high aluminium incorporation causes ''flaking-off'' of Al atoms from tetrahedral sites in the mesoporous walls to octahedral and pentahedral sites. The pentahedrally coordinated Al is indicative of the defects of grafted Al phase.[18] Pt/HAlMSN-7 showed 4-, 5- and 6-coordinated Al structures while the other samples exhibited 4- and 5-coordination. Consequently, the generation of non-acidic Al structure in the Al-rich sample is probably due to the presence of paired framework Al atoms and five-coordinated aluminium located at the interface between the tetrahedral aluminosilicate framework and the octahedral alumina phase.[19]

Similarly, Bhange *et al.*[20] reported the modification of SBA-15 by loading various amounts of aluminium which led to the observation of octahedrally, pentahedrally and tetrahedrally coordinated Al structures at 1, 30 and 52–54 ppm, respectively.

FTIR spectra of the Pt/HAlMSN catalysts in the range of 3800–3500 cm^{-1} are shown in Fig. 4A.

The sharp band at 3740 cm^{-1} is assigned to the non-acidic isolated silanol hydroxyl groups (Si–OH) observed on the

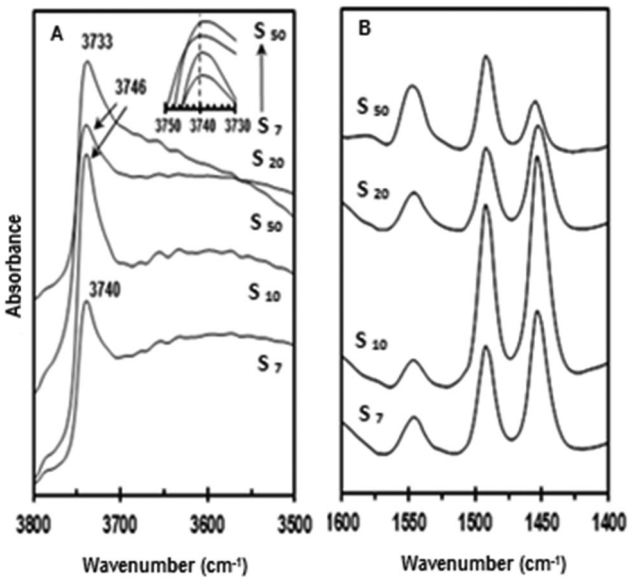

Fig. 4 (A) FTIR spectra of the Pt/HAlMSN catalysts with Si/Al ratios of 7–50 for the hydroxyl group stretching region at 3500–3800 cm^{-1}; (B) pyridine adsorption FTIR spectra of Pt/HAlMSN with Si/Al ratios of 7–50. Pyridine was adsorbed at 423 K for 30 min, followed by outgassing at 473 K for 1 h.

external surface of mesoporous catalysts.[21] A decrease in the H-bonds of hydroxyl groups is evidence for the increase in the substitution of Al atoms into the framework. These silanol groups were observed inside the channels and were connected with structural imperfections or local defects.[21]

IR spectra of the Pt/HAlMSN catalysts also showed the bridge hydroxyl group of Si–OH–Al at 3552 and 3637 cm^{-1} which is assigned to the framework Al atom. The broad band at 3660 cm^{-1} is assigned to the presence of Si–OH–Al···Al structure and shows the interaction of the OH group with extra-framework Al which is assigned to the presence of an octahedral Al atom.[22]

The peak observed at 3520 cm^{-1} illustrated the hydrogen-bonded internal Si–OH groups which decreased with more aluminium grafting. The peak at 3580 cm^{-1} is assigned to H-bonded OH and described the weak acidic property.[22]

Brønsted and Lewis acidity in the Pt/HAlMSN solid catalysts

The effect of Si/Al ratio and temperature was observed in the acidity of the catalysts. The number of acid sites was altered by the aluminium concentration. The number of Lewis acid sites increased and the number of Brønsted acid sites decreased with the increase in Al content and temperature. An increase in temperature enhanced the removal of hydrogen from the Brønsted acid sites which led to a decrease in these sites and an increase in Lewis acidity.

Fig. 4B shows the acidity of Pt/HAlMSN which adsorbed pyridine at room temperature, followed by evacuation at 673 K. The pyridine-IR spectrum at 423 K shows the Lewis and Brønsted acid sites at 1455 and 1545 cm^{-1}, respectively. An increase in Lewis acid sites indicates an increase in Al concentration due to the replacement of Al species with Si atoms. Tetrahedrally coordinated Al^{3+} ions were responsible for Lewis acid sites formed through the isomorphous substitution of Si^{4+} lattice sites by Al^{3+} ions, leading to the generation of an aluminosilicate phase.[23] The relationship between the framework Al concentration and acid strength may be explained by the presence of Al atoms in the second neighbor which can be supposed to have increased Lewis acidity.[18] The presence of tetrahedral and octahedral Al structures in these catalysts which are responsible for the Lewis and Brønsted acid sites, respectively, was confirmed by ^{27}Al MAS NMR and pyridine adsorption FTIR spectra.

Wang *et al.*[17] reported the synthesis of a low-silica AlMCM-41 with Si/Al = 1.25 and studied the gradual collapse in their frameworks during the dealumination process. The fraction of tetrahedral Al in the solid decreased with the level of dealumination. The presence of platinum on these catalysts did not significantly modify the intensity of Brønsted and Lewis bands. The acidic properties of platinum loaded nanoparticles did not directly influence the hydrocracking activity.[24] The Brønsted acid strength decreased and Lewis acidity increased with the increase in Al content.

Fig. 5A–D show IR spectra of the Pt/HAlMSN samples which were activated at 473, 523, 573 and 623 K for 3 h, then pyridine was adsorbed at 423 K for 30 min, followed by outgassing at 473 K. Fig. 5E and F illustrate variation of the intensity of Lewis and Brønsted acid sites determined by pyridine desorption. The number of Lewis acid sites increased (Fig. 5E) while Brønsted acid sites decreased (Fig. 5F) with the rise in temperature. Pt/HAlMSN-7 showed less Lewis acidity than Pt/HAlMSN-10 due to the presence of inactive framework Al structure in this catalyst. A decrease in the Brønsted acid sites indicates the removal of hydrogen with temperature and the subsequent increase in the number of Lewis acid sites.

Measurement of molar absorption coefficients of the Pt/HAlMSN catalysts

The activity of the catalysts is related to the ratio of Brønsted acid sites to Lewis acid sites ([B]/[L]).[25] Using pyridine followed by water adsorption monitored by infrared spectroscopic techniques is a method to measure the strength of Brønsted and Lewis acid sites.[25]

Water is absorbed on Lewis acid sites selectively and it forms hydroxyl groups as Brønsted acid sites on the surface of the sample. This method changes all the physically adsorbed pyridine on Lewis acid sites to chemically adsorbed pyridinium ions on Brønsted acid sites.[25]

The molar absorption coefficient of pyridinium ions on Brønsted acid sites at 1545 cm^{-1} (ε_{B1545}), and the molar absorption coefficient of pyridinium ions on Brønsted acid sites and pyridine on Lewis acid sites at 1490 cm^{-1} (ε_{B1490}, ε_{L1490}) were calculated. If [B] indicates the amount of pyridinium ions bound to Brønsted acid sites and [L] the amount of pyridine bound to Lewis acid sites, the ratio of [B]/[L] can be expressed as

$$[B]/[L] = A_{1545}/(A_{1545}' - A_{1545}) \quad (3)$$

where A_{1545} and A_{1545}' are the intensities of the bands at 1545 cm^{-1} before and after the adsorption of water, respectively. The molar absorption coefficient of pyridinium ions on Brønsted acid sites at

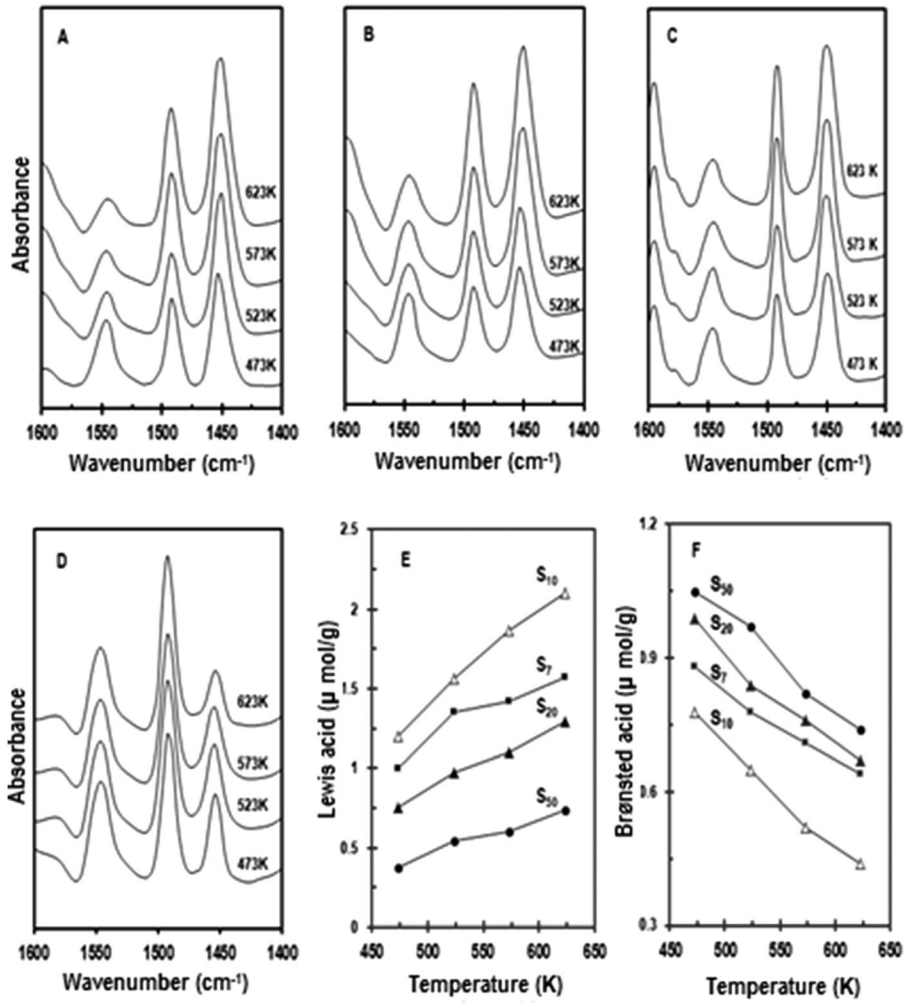

Fig. 5 IR spectrum of Pt/HAlMSN samples with Si/Al ratios of 7 (A), 10 (B), 20 (C) and 50 (D) which were activated at 473, 523, 573 and 623 K for 3 h, then pyridine were adsorbed at 423 K for 30 min, followed by outgassing at 473 K; variations of the absorbance of IR acid sites (Lewis (E) and Brønsted (F)) with the activated temperatures. Samples were activated at 473, 523, 573 and 623 K for 3 h. Pyridine was adsorbed at 423 K for 30 min, followed by outgassing at 473 K.

1545 and 1490 cm^{-1} and that of pyridine on Lewis acid sites at 1490 cm^{-1} were denoted as ε_{1545}, ε_{B1490} and ε_{L1490} were obtained as follows:

$$A_{1545} = \varepsilon_{1545}[B] \quad (4)$$

$$A_{1490} = \varepsilon_{B1490}[B] + \varepsilon_{L1490}[L] \quad (5)$$

The ratio of the molar absorption coefficient of pyridinium ions on the band at 1490 to 1545 cm^{-1} will be

$$\varepsilon_{B1490}/\varepsilon_{1545} = A_{1490}'/A_{1545}' \quad (6)$$

$$\varepsilon_{B1490}[B] = (\varepsilon_{B1490}/\varepsilon_{1545})A_{1545} \quad (7)$$

From eqn (4), (5) and (7), $\varepsilon_{B1490}[B]$ and $\varepsilon_{L1490}[L]$ can be expressed as

$$\varepsilon_{B1490}[B]/\varepsilon_{L1490}[L] = (\varepsilon_{B1490}/\varepsilon_{L1490})([B]/[L]) \quad (8)$$

$$\varepsilon_{B1490}/\varepsilon_{L1490} = (A_{1490}'/A_{1545}')(A_{1545}' - A_{1545})/\{A_{1490} - (A_{1490}'/A_{1545}')A_{1545}\} \quad (9)$$

If X_B and X_L were attributed to pyridine adsorbed on Brønsted and Lewis acid sites respectively, the intensities of the bans at 1490 and 1545 cm^{-1} were obtained as follows:

$$A_{1490} = \varepsilon_{B1490}X_B + \varepsilon_{L1490}X_L \quad (10)$$

$$A_{1545} = \varepsilon_{1545}X_B \quad (11)$$

The intensities of the bands at 1490 and 1545 cm^{-1} were measured as

$$A_{1490}' = \varepsilon_{B1490}(X_B + X_B') + \varepsilon_{L1490}(X_L + X_L') \quad (12)$$

$$A_{1545}' = \varepsilon_{1545}(X_B + X_B') \quad (13)$$

From eqn (10) to eqn (13), $\varepsilon_{B1490}/\varepsilon_{L1490}$ and $\varepsilon_{B1490}/\varepsilon_{1545}$ and the molar absorption coefficient of ε_{B1490}, ε_{L1490}, ε_{1545} can be calculated. The molar absorption coefficient units, ε, were measured by using Beer–Lambert law equation:

$$A = (\varepsilon \times n)/S \quad (14)$$

where A (cm^{-1}), ε (cm μmol^{-1}), n (mole) and S ($cm^2\ g^{-1}$) denote respectively the absorbance, the molar absorption coefficient,

Table 2 The molar absorption coefficients for absorption bands at 1550–1545 cm^{-1} (Brønsted sites, ε_B), 1455–1450 cm^{-1} (Lewis sites, ε_L) and the amount of Brønsted and Lewis acid sites in this study and reported in the literature

Catalyst	ε_B [a]	ε_L [a]	[B]/[L]	Ref.
Pt/HAlMSN-7	1.26	2.08	0.34	This study
Pt/HAlMSN-10	1.49	1.57	0.40	This study
Pt/HAlMSN-20	1.03	1.40	1.12	This study
Pt/HAlMSN-50	1.15	2.17	0.35	This study
Silica–alumina	0.56	1.44	—	26
SiO_2, Al_2O_3	1.80–2.20	—	—	27
Zeolite, ASA	1.67	2.22	—	28
Si–Zr (0.2 *in situ*)	0.77	2.08	—	30
Si–Zr (9 mol%)	1.32	1.49	—	30
Si–Zr (20 mol%)	1.16	1.58	—	30

[a] IR absorption coefficient (cm μmol^{-1}).

the amount of pyridine adsorbed and the surface of the pressed disk. Calculated molar absorption coefficients for Brønsted and Lewis acid sites in the Pt/HAlMSN catalysts at 1490 and 1545 cm^{-1} and some reported molar absorption coefficients for different solid catalysts are shown in Table 2. These studies have reported the molar absorption coefficient using a regression analysis of pyridine adsorption FTIR at 423 K with different Si/Al solid catalysts and the results of these studies are in good agreement with our results. The calculated values for the pyridine ion (Brønsted sites with the corresponding band at 1545 cm^{-1}) varied within the range 0.56–2.2 cm μmol^{-1} and for Lewis acid sites the average values of ε were 1.44 and 2.22 cm μmol^{-1}.[26–30]

Influence of the Si/Al molar ratio and platinum on cumene conversion and selectivity

The influence of the Si/Al molar ratio on the cumene hydrocracking over Pt/HAlMSN in the region of 323–523 K is shown in Fig. 6A. The cumene hydrocracking was enhanced with increasing temperature which suggested that the catalytic activity directly depends on the temperature and Al concentration. An increase in Al content increased the catalytic activity through an increase in catalyst acidity. The bifunctional catalysts of Pt/HAlMSN showed a high activity of 84, 88, 97 and 94% for Si/Al ratios of 50–7, respectively, at 523 K. Generally, the presence of platinum in the heterogeneous catalyst promotes the conversion of cumene cracking.[31] According to the published reports, at 523 K, the cumene cracking over the monofunctional catalyst of Al-MCM-41 (Si/Al = 20)[32] and Pt-supported MCM-41[33] was 13.5 and 25.1%, respectively, while the bifunctional catalyst of Pt/HAlMSN represented 88% cumene conversion.

According to the previous study,[2] the cumene conversion over the monofunctional catalyst of HAlMSN (Si/AL = 20) was 55%, while this conversion was 88% for Pt/HAlMSN (Si/Al = 20) at 523 K. Therefore, the presence of Pt species plays a significant role in promoting cumene conversion.[34]

The results showed that the catalytic activity of these samples was influenced by the presence of acid sites accompanied by Pt species. The platinum sites protect the neighbouring acid sites from deactivation within a determined radius, through the hydrogen spillover process.[24] Hydrogen molecules were adsorbed

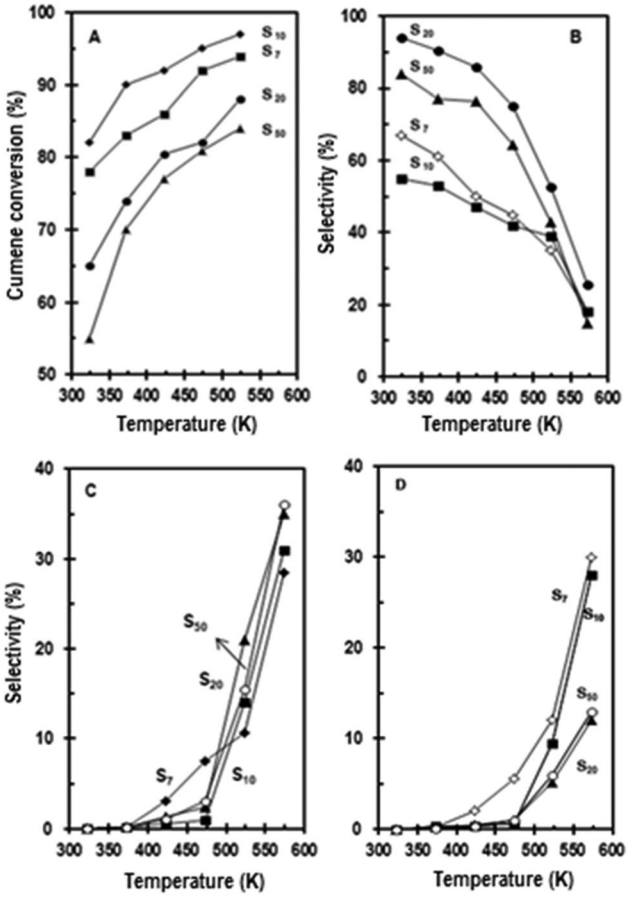

Fig. 6 (A) Relationship between the Si/Al molar ratio and cumene conversion in the region of 323, 373, 423, 473 and 523 K; the selectivity of (B) α-methylstyrene, (C) propene and (D) benzene formation over the Pt/HAlMSN catalysts.

on Pt sites of the catalysts and generated hydrogen atoms which spillover onto the surface of Pt/HAlMSN and undergo surface diffusion. The hydrogen reaches a Lewis acid center and donates an electron to form H^+ which is stabilized on an oxygen atom near the Lewis acid sites. The Lewis acid site traps an electron which then reacts with the second spillover hydrogen to form an H^- bond with a Lewis acid site.[34]

Fig. 6A also shows the influence of temperature on cumene conversion and selectivity over the Pt/HAlMSN catalysts. The conversion of cumene reaction increased with increasing temperature from 323 to 523 K in a relatively regular manner. The maximum conversion of 84, 88, 97 and 94% was observed at 523 K over Pt/HAlMSN with ratios of 50–7, respectively. The results showed that the generation of pentahedrally coordinated Al structure in Pt/HAlMSN-7 decreased the activity of this catalyst in comparison with Pt/HAlMSN-10.

The major products of cumene cracking over Pt/HAlMSN were composed of propene, benzene, toluene and α-methylstyrene. The high activity of cumene conversion was due to the presence of molecular hydrogen and strong Lewis acid sites in which the strong Lewis acid sites act as active sites for the formation of protonic acid sites. The protonic acid sites were responsible for

the production of propene, benzene and toluene *via* the dealkylation process, while the strong Lewis acid sites enhanced the dehydrogenation process and produced α-methylstyrene.[35,36] The presence of platinum accelerated the cracking of cumene reaction.

In agreement with the obtained results, Corma *et al.* stated that the Brønsted acid sites in the cracking of cumene are responsible for the generation of carbenium ions which lead to the formation of propene and benzene.[37] The presence of the strong Lewis acid sites accelerates the hydride transfer which enhances the formation of α-methylstyrene. Bradley and Kydd studied the cracking reaction of iso-propyl benzene with an alumina supported gallium catalyst to produce propene and α-methylstyrene through solid catalyzed dehydrogenation and cracking reactions.[35] Cumene dehydrogenation has also been explored over complex-derived Cr- and Fe–Cr-pillared clays in which the products of benzene and propene were produced at low temperature, and α-methylstyrene was observed at higher temperatures.[36]

Fig. 6B–D shows the selectivity of α-methylstyrene, propene and benzene as the selected products of cumene conversion in the range of 323–573 K in a microcatalytic pulse reactor under a hydrogen carrier gas. In all catalysts, α-methylstyrene was produced due to the predominant effect of Lewis acid sites during the dehydrogenation mechanism which reduced with increasing temperature. The selectivity of α-methylstyrene is 75, 65, 45 and 42%, respectively, at 473 K, for the samples with Si/Al ratios of 20, 50, 7 and 10. The order of α-methylstyrene formation is due to the number of Lewis acid sites in the catalysts. The amount of α-methylstyrene decreased with the increase of temperature. Therefore, α-methylstyrene selectivity decreased with a decrease in the number of Lewis acid sites in accordance with the Si/Al ratio of 20 > 50 > 7 > 10. The amounts of propene and benzene gradually increased with temperature which confirmed the role of protonic acid sites.

The mechanisms of cumene cracking were proposed in terms of the generated ions due to the operation of Lewis and Brønsted acid sites. The formation of α-methylstyrene in cumene hydrocracking is attributed to Lewis acidity, according to the dehydrogenation mechanism (Scheme 1). This mechanism of cumene conversion involves several modes: firstly, the Lewis acid attaches to the aromatic ring and generates a cation site; secondly, the C–H bond of the methyl group undergoes cleavage and then the hydrogen shifts from the methine group of propyl to the cation site in order to neutralize the positive charge; finally, the Lewis acid and hydrogen molecule separate and then form α-methylstyrene in which the separated Lewis acid will be applied for establishing a new attachment to the aromatic carbon.[38]

Another mechanism is based on the generation of carbenium ions in cumene conversion reaction which lead to the formation of propene and benzene attributed to the interaction of the protonic acid site generated from molecular hydrogen. The mechanism of dealkylation is ascribed to the operation of the Brønsted acid sites on the surface of catalysts (Scheme 2). This mechanism of cumene cracking includes the following steps: (1) protonation at the aromatic carbon in which the isopropyl group is attached, (2) generation of a propyl cation and benzene compound and (3) deprotonation of the propyl cation to produce propene and protons which will be applied for the protonation at the aromatic carbon.[39]

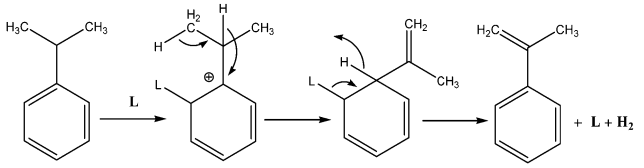

Scheme 1 Mechanism of α-methylstyrene formation (dehydrogenation process) on Lewis acid sites of the Pt/HAlMSN catalysts.[38]

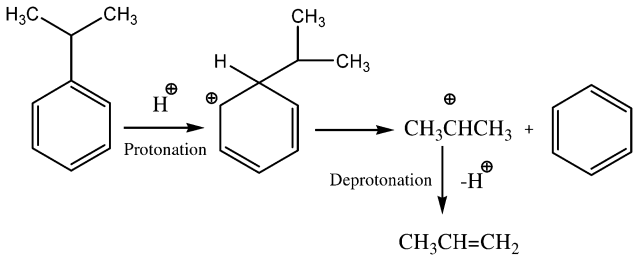

Scheme 2 Mechanism of propene and benzene formation (dealkylation process) on the Brønsted acid sites of the Pt/HAlMSN catalysts.[39]

Influence of temperature on cumene conversion and product selectivity

Fig. 6 also shows the influence of temperature on cumene conversion and selectivity over the Pt/HAlMSN catalysts. The conversion of cumene reaction increased with increasing temperature from 323 to 523 K in a relatively regular manner. An increase of the catalytic activity with increasing temperature over these bifunctional catalysts is evidence for the spillover phenomenon due to the presence of platinum species.[7] In this process the molecules of hydrogen dissociate on Pt particles and react with cumene molecules on the surface acid sites and application of higher temperature increases the spillover process on the surface active sites. Using higher temperature increases the spillover process on the surface active sites.[7] This indicates the effect of Al species as a co-promoting agent for active Pt sites. The cumene conversion trend is similar to the operation of Lewis acid sites.

The role of acid sites in cumene conversion

The role of acidic sites was strongly evidenced by the activity–acidic site relationship which is shown in Fig. 7. The ratio of the cumene conversion to the concentration of Lewis acid sites gradually changed in the temperature range of 473–573 K, while the ratio of the concentration to the Brønsted acid sites was more altered. In fact, the slope of the lines related to the Brønsted acid sites is more in comparison with that of the Lewis acid site.

This result indicated that the cumene conversion is more correlated with the concentration of Lewis acid sites in which the Lewis acid sites have important roles in the stabilization of the formed protons and in facilitating the dehydrogenation

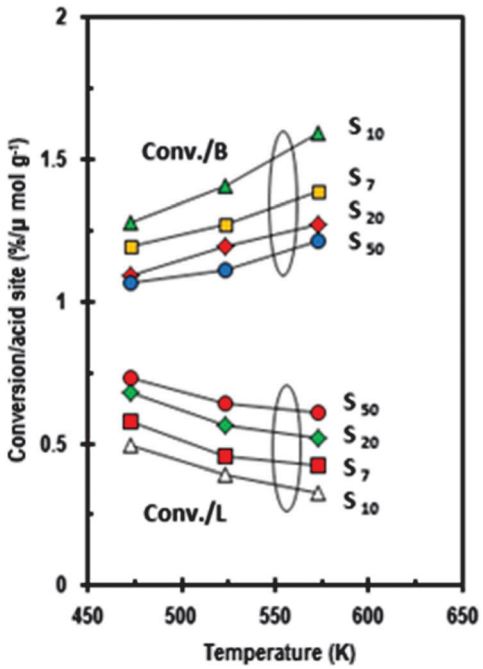

Fig. 7 The relation between cumene conversion and the number of acidic sites at 473–573 K.

process. Thus, according to the obtained results, the high activity of Pt/HAlMSN is due to the number of Lewis acid sites. On the other hand, the presence of permanent Brønsted acid sites cannot be directly associated with the cumene conversion activity over Pt/HAlMSN.[2] In fact, the cumene conversion was low in the absence of molecular hydrogen.

Table 3 shows a comparative study of cumene conversion over several types of solid catalysts such as Pt/HAlMSN, HAlMSN,[2] commercial γ-Al_2O_3,[2] 20-Al-MCM-41,[40] Al-SBA-15(Si/Al=20),[9] HMFI-SBA-15,[41] Pt/SiO_2 mixed with H-β,[42] FSM-Al-7.8,[43] Pt/Al-SBA-15[11] and Pt/Al_2O_3-MCM-41.[33] The results show that the activity of Pt/HAlMSN for cumene conversion is higher than the other catalysts at the same or close to the same temperature. The reason probably is due to the presence of extra-framework aluminium which generates strong Lewis acid sites[2] and the presence of platinum species which provides more interaction between active sites and reactant or hydrogen carrier gas through the spillover phenomenon.

Stability testing

The stability tests of all catalysts are shown in Fig. 8, where the cumene conversion (%) is plotted as a function of time (h). The conversions of cumene were 94, 97, 88 and 84% for Pt/HAlMSN with Si/Al ratios of 7 to 50 at 523 K, respectively. The activity of these catalysts was studied for more than 100 h.[44] The activities were found to slightly decrease with the reaction time for more than 100 h. After stability testing, all spent catalysts were subjected to XRD and FTIR in order to study their properties.

XRD results (not shown) indicated that there is no significant change after the reaction; however, coke deposits were observed on the used catalysts. The strong distinctive band

Table 3 The activity of cumene conversion over Pt/HAlMSN and other types of solid acid catalysts in the presence of hydrogen gas

Catalyst	Cumene conv. (%)	Temp. (K)	Ref.
Pt/HAlMSN-50	84	523	This study
Pt/HAlMSN-20	88	523	This study
Pt/HAlMSN-10	97	523	This study
Pt/HAlMSN-7	94	523	This study
HAlMSN-20	55	523	2
Commercial γ-Al_2O_3	Trace	523	2
Al-SBA-15 (Si/Al = 20)	17.1	523	9
20-Al-MCM-41	13.5	573	40
5-Al-MCM-41	3.4	673	9
HMFI-SBA-15	15	573	41
Pt/SiO_2 + H-beta	30	503	42
FSM-Al-7.8	26.7	673	43
Pt/Al-SBA-15	Trace	573	11
Pt/Al_2O_3-MCM-41	31.2	523	33

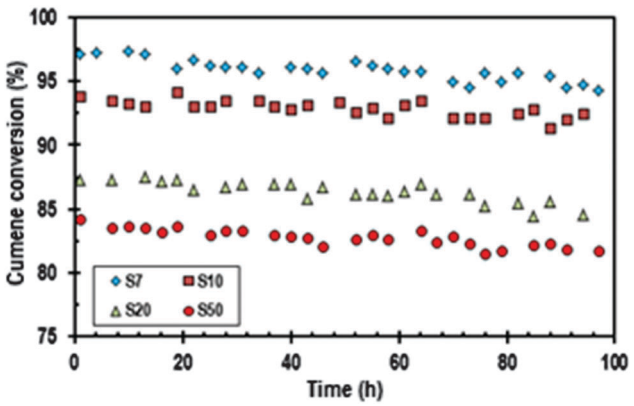

Fig. 8 Stability test of the Pt/HAlMSN catalysts at a reaction temperature of 523 K.

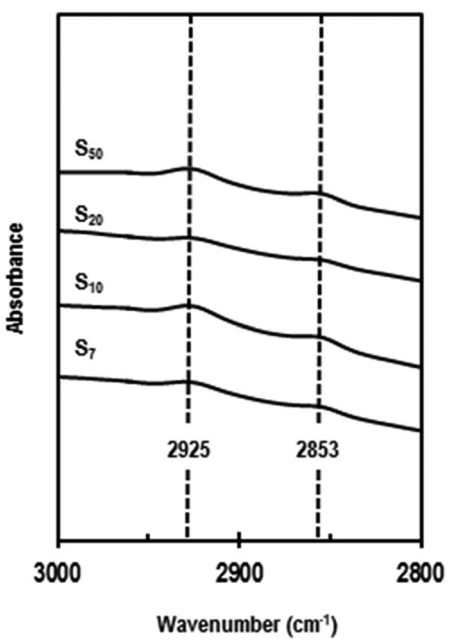

Fig. 9 FTIR spectra of the used Pt/HAlMSN; cumene conversion was done at 523 K in the presence of hydrogen stream.

corresponds to the vibration of C=C observed at 1645 cm^{-1}, which may be related to the presence of olefinic species.[2] In addition, two weak bands observed at 2850 and 2925 cm^{-1} confirmed the presence of the C–H stretching vibration, which is related to the aliphatic hydrocarbons (Fig. 9).

These results show that the decrease in activity may be due to the undesirable carbon deposition on the pores of catalysts during the cumene conversion. The coke formation has a little effect on the activity of the catalysts. This probably indicates that the high activity may be due to the large amount of active surface area and pore size which still remained after 100 h of reaction.

Conclusion

The effects of the Si/Al molar ratio on the properties and activity of Pt/HAlMSN in cumene cracking were studied by using different Si/Al molar ratios of 7, 10, 20 and 50. XRD and N_2 physisorption results indicated that the increase in the Si/Al ratio enhanced the percentage crystallinity and hexagonal ordered structures of the catalysts. This led to reduction of specific surface area from 775 $m^2 g^{-1}$ for Pt/HAlMSN with a Si/Al ratio of 50 to 361 $m^2 g^{-1}$ for Pt/HAlMSN with a Si/Al ratio of 7. The pore volume also decreased from 0.40 to 0.15 $cm^3 g^{-1}$ and the pore diameter decreased from 3.77 to 3.64 nm for the Si/Al ratio of 50 to 7, respectively. ^{27}Al and ^{29}Si solid state NMR and IR spectroscopy results indicated that a decrease in the Si/Al ratio changed the structures, which led to the generation of strong Brønsted and Lewis acidic sites.

^{27}Al NMR confirmed the presence of tetrahedral, pentahedral and octahedral aluminium structures which 5-coordinated aluminium structure observed only in Pt/HAlMSN-7. Pyridine adsorption FTIR results showed that an increase in the Si/Al ratio decreased the number of acid sites which led to a decrease in the catalytic activity towards cumene conversion.

Cumene conversion over these catalysts revealed an increase in cracking from Si/Al molar ratios of 50 to 10 (from 84 to 97%) and a decrease in Pt/HAlMSN with a Si/Al molar ratio of 7 (94%) due to the presence of pentahedral aluminium and/or inactive tetrahedral aluminium atoms. The mechanism of dehydrogenation on Lewis acid sites is responsible for α-methylstyrene formation and the dealkylation process produces propene, benzene, and toluene *via* cracking on protonic acid sites through the Brønsted acidity.

The stability test showed that although the coke formation could gradually affect the activity of these catalysts, the large active surface area and pore size still remained after 100 h of reaction.

The molar absorption coefficient of Pt/HAlMSN samples was calculated using pyridine followed by water adsorption examined by FTIR spectroscopy which is a technique to measure the strength of Brønsted and Lewis acid sites in the catalysts.

Acknowledgements

This work was supported by the Universiti Teknologi Malaysia under RUG Project No. 06H17. Our gratitude also goes to the Hitachi Scholarship Foundation, Japan, for the Gas Chromatograph Instruments Grant.

References

1 J. S. Beck, J. C. Vartuli, W. J. Roth, M. E. Leonowicz, C. T. Kresge, K. D. Schmitt, C. T. W. Chu, D. H. Olson, E. W. Sheppard, S. B. Mc Cullen, J. B. Higgins and J. L. Schlenker, *J. Am. Chem. Soc.*, 1992, **114**, 10834.
2 M. R. Sazegar, A. A. Jalil, S. Triwahyono, R. R. Mukti, M. Aziz, M. A. A. Aziz, N. H. N. Kamarudin and H. D. Setiabudi, *Chem. Eng. J.*, 2014, **240**, 352.
3 J. H. Clark, D. J. Macquarrie and S. J. Tavener, *Dalton Trans.*, 2006, 4297.
4 M. A. A. Aziz, A. A. Jalil, S. Triwahyono, R. R. Mukti, Y. H. Taufiq-Yap and M. R. Sazegar, *Appl. Catal., B*, 2014, **147**, 359.
5 K. O'Malley, A. Gil and T. Curtin, *Microporous Mesoporous Mater.*, 2012, **191**, 48.
6 N. H. N. Kamarudin, A. A. Jalil, S. Triwahyono, M. R. Sazegar, S. Hamdan, S. Baba and A. Ahmad, *RSC Adv.*, 2015, **5**, 30023.
7 H. D. Setiabudi, A. A. Jalil and S. Triwahyono, *J. Catal.*, 2012, **294**, 128.
8 N. H. N. Kamarudin, A. A. Jalil, S. Triwahyono, M. R. Sazegar, S. Hamdan, S. Baba and A. Ahmad, *RSC Adv.*, 2015, **5**, 30023.
9 S. K. Jana, H. Takahashi, M. Nakamura, M. Kaneko, R. Nishida, H. Shimizu, T. Kugita and S. Namba, *Appl. Catal., A*, 2003, **245**, 33.
10 H. M. Moura and H. O. Pastore, *Dalton Trans.*, 2014, **43**, 10471.
11 S. Handjani, S. Dzwigaj, J. Blanchard, E. Marceau, J. M. Krafft and M. Che, *Top. Catal.*, 2009, **52**, 334.
12 N. N. Ruslan, S. Triwahyono, A. A. Jalil, S. N. Timmiati and N. H. R. Annuar, *Appl. Catal., A*, 2012, **413–414**, 176.
13 C. T. Kresge, M. E. Leonowiez, W. J. Roth and J. C. Vartuli, *US Pat.*, 5,098,684, 1992.
14 L. Y. Chen, Z. Ping, G. K. Chuah, S. Jaenicke and G. Simon, *Microporous Mesoporous Mater.*, 1999, **27**, 231.
15 J. Liu, L. Zhang, Q. Yang and C. Li, *Microporous Mesoporous Mater.*, 2008, **116**, 330.
16 F. Subhan and B. S. Liu, *Chem. Eng. J.*, 2011, **178**, 69.
17 Y. Wang, N. Lang and A. Tuel, *Microporous Mesoporous Mater.*, 2006, **93**, 46.
18 X. W. Cheng, Q. P. He, J. Guo, H. Yan, H. Y. He and Y. C. Long, *Microporous Mesoporous Mater.*, 2012, **149**, 10.
19 B. M. De Witte, P. J. Grobet and J. B. Uytterhoeven, *J. Phys. Chem.*, 1995, **99**, 6961.
20 P. Bhange, D. S. Bhange, S. Pradhan and V. Ramaswamy, *Appl. Catal., A*, 2011, **400**, 176.
21 M. Bevilacqua, T. Montanari, E. Finocchio and G. Busca, *Catal. Today*, 2006, **116**, 132.
22 A. Jentys, N. H. Pham and H. Vinek, *J. Chem. Soc., Faraday Trans.*, 1996, **92**, 3287.
23 W. Daniell, U. Schubert, R. Glöckler, A. Meyer, K. Noweck and H. Knözinger, *Appl. Catal., A*, 2000, **196**, 247.
24 T. N. Vu, J. van Gestel, C. Collet, J. P. Dath and J. C. Duchet, *J. Catal.*, 2005, **231**, 453.

25 P. Alexandru and J. T. William, *Ind. Eng. Chem. Res.*, 2003, **42**, 5988.
26 I. S. Pieta, M. Ishaq, R. P. K. Wells and J. A. Anderson, *Appl. Catal., A*, 2010, **390**, 127.
27 T. Onfroy, G. Clet and M. Houalla, *Microporous Mesoporous Mater.*, 2005, **82**, 99.
28 C. A. Emeis, *J. Catal.*, 1993, **141**, 347.
29 D. J. Rosenberg, B. B. Baeza, T. J. Dines and J. A. Anderson, *J. Phys. Chem. B*, 2003, **107**, 6526.
30 D. J. Rosenberg and J. A. Anderson, *Catal. Lett.*, 2002, **83**, 59.
31 B. Wang, X. Wu, R. Ran, Z. Si and D. Weng, *J. Mol. Catal. A: Chem.*, 2012, **361–362**, 98–103.
32 R. Mokaya, W. Jones, Z. Luan, M. D. A. Klinowski and J. Klinowski, *Catal. Lett.*, 1996, **37**, 113.
33 Y. Kanda, T. Kobayashi, Y. Uemichi, S. Namba and M. Sugioka, *Appl. Catal., A*, 2006, **308**, 111.
34 S. N. Timmiati, A. A. Jalil, S. Triwahyono, H. D. Setiabudi and N. H. R. Annuar, *Appl. Catal., A*, 2013, **459**, 8.
35 S. M. Bradley and R. A. Kydd, *J. Catal.*, 1993, **141**, 239.
36 T. Mishra and K. Parida, *Appl. Catal., A*, 1998, **174**, 91.
37 A. Corma, P. J. Miguel and A. V. Orchilles, *J. Catal.*, 1994, **145**, 58.
38 A. Corma and B. W. Wojciechowski, *Catal. Rev.: Sci. Eng.*, 1982, **24**, 1.
39 N. H. R. Annuar, A. A. Jalil, S. Triwahyono, N. A. A. Fatah, L. P. The and C. R. Mamat, *Appl. Catal., A*, 2014, **475**, 487.
40 D. Trong On, S. M. J. Zaidi and S. Kaliaguine, *Microporous Mesoporous Mater.*, 1998, **22**, 211.
41 R. Contreras, J. Ramirez, R. Cuevas-Garci, A. Gutierrez-Alejandre, P. Castillo-Villalon, G. Macias and I. Puente-Lee, *Catal. Today*, 2009, **148**, 49.
42 T. Kusakari, K. Tomishige and K. Fujimoto, *Appl. Catal., A*, 2002, **224**, 219.
43 K. Hamaguchi and H. Hattori, *React. Kinet. Catal. Lett.*, 1997, **61**, 13.
44 M. A. A. Aziz, A. A. Jalil, S. Triwahyono and M. W. A. Saad, *Chem. Eng. J.*, 2015, **260**, 757.

